Journal of Hydrology 524 (2015) 625–641

Contents lists available at ScienceDirect

Journal of Hydrology

journal homepage: www.elsevier.com/locate/jhydrol

Effects of anthropogenic groundwater exploitation on land surface processes: A case study of the Haihe River Basin, northern China

Jing Zou [a,b], Zhenghui Xie [a,*], Chesheng Zhan [c], Peihua Qin [a], Qin Sun [a], Binghao Jia [a], Jun Xia [c]

[a] State Key Laboratory of Numerical Modeling for Atmospheric Sciences and Geophysical Fluid Dynamics, Institute of Atmospheric Physics, Chinese Academy of Sciences, Beijing 100029, China[1]

[b] Institute of Oceanographic Instrumentation, Shandong Academy of Sciences, Qingdao 266001, China

[c] Key Laboratory of Water Cycle and Related Land Surface Processes, Institute of Geographic Sciences and Natural Resources Research, Chinese Academy of Sciences, Beijing 100101, China

ARTICLE INFO

Article history:
Received 11 July 2014
Received in revised form 4 March 2015
Accepted 7 March 2015
Available online 19 March 2015
This manuscript was handled by Konstantine P. Georgakakos, Editor-in-Chief, with the assistance of Michael Bruen, Associate Editor

Keywords:
Groundwater exploitation
Land surface process
Haihe River Basin

SUMMARY

In this study, we incorporated a groundwater exploitation scheme into the land surface model CLM3.5 to investigate the effects of the anthropogenic exploitation of groundwater on land surface processes in a river basin. Simulations of the Haihe River Basin in northern China were conducted for the years 1965–2000 using the model. A control simulation without exploitation and three exploitation simulations with different water demands derived from socioeconomic data related to the Basin were conducted. The results showed that groundwater exploitation for human activities resulted in increased wetting and cooling effects at the land surface and reduced groundwater storage. A lowering of the groundwater table, increased upper soil moisture, reduced 2 m air temperature, and enhanced latent heat flux were detected by the end of the simulated period, and the changes at the land surface were related linearly to the water demands. To determine the possible responses of the land surface processes in extreme cases (i.e., in which the exploitation process either continued or ceased), additional hypothetical simulations for the coming 200 years with constant climate forcing were conducted, regardless of changes in climate. The simulations revealed that the local groundwater storage on the plains could not contend with high-intensity exploitation for long if the exploitation process continues at the current rate. Changes attributable to groundwater exploitation reached extreme values and then weakened within decades with the depletion of groundwater resources and the exploitation process will therefore cease. However, if exploitation is stopped completely to allow groundwater to recover, drying and warming effects, such as increased temperature, reduced soil moisture, and reduced total runoff, would occur in the Basin within the early decades of the simulation period. The effects of exploitation will then gradually disappear, and the variables will approach the natural state and stabilize at different rates. Simulations were also conducted for cases in which exploitation either continues or ceases using future climate scenario outputs from a general circulation model. The resulting trends were almost the same as those of the simulations with constant climate forcing, despite differences in the climate data input. Therefore, a balance between slow groundwater restoration and rapid human development of the land must be achieved to maintain a sustainable water resource.

1. Introduction

As an essential part of the hydrological cycle, groundwater plays an important role in sustaining streams, lakes, wetlands, and aquatic communities (Alley et al., 2002). It is also a crucial source of freshwater for industrial manufacturing, domestic use, agricultural irrigation, and other activities throughout the world. With population growth and economic development, the disparity between the supply of and demand for water resources is becoming increasingly serious, and people exploit groundwater to meet local water demands (Xia and Chen, 2001; Sha et al., 2003; Xia and Zhang, 2008). However, groundwater exploitation has various negative effects on the land surface, including the depletion of local water resource, a weakening of the hydraulic connections between

* Corresponding author at: State Key Laboratory of Numerical Modeling for Atmospheric Sciences & Geophysical Fluid Dynamics (LASG), Institute of Atmospheric Physics, Chinese Academy of Sciences, P.O. Box 9804, Beijing 100029, China. Tel.: +86 10 82995179 (O); fax: +86 10 82995172 (O).
E-mail address: zxie@lasg.iap.ac.cn (Z. Xie).
[1] http://www.lasg.ac.cn/staff/xie/xie.htm.

http://dx.doi.org/10.1016/j.jhydrol.2015.03.026
0022-1694/

aquifers and rivers, and changes in the local heat flux and moisture flux responses at the land surface (Koster and Suarez, 2001; Chen and Hu, 2004; Yuan et al., 2008; Kustu et al., 2010). As excessive groundwater exploitation becomes a growing problem globally, it is necessary to understand the effects of groundwater exploitation on local hydrological processes and regional climates (Konikow and Kendy, 2005; Rodell et al., 2009; Wada et al., 2010, 2012; Zou et al., 2014).

Many hydrological studies based on observations or simulations have been undertaken to determine the relationships between a lowered water table and changes in the stream flow in river basins (Ren et al., 2002; Kollet and Zlotnik, 2003; Wen and Chen, 2006; Chen et al., 2008; Hanasaki et al., 2008; Döll et al., 2012). Szilagyi (1999, 2001) found the significant depletion of the stream flow in the Republican River Basin, USA, resulted from agricultural irrigation and other human groundwater-consuming activities. The climatic effects of irrigation which constitutes the greatest component of water consumption by human activity have also been investigated (Haddeland et al., 2006; Kueppers et al., 2007; Chen and Xie, 2010). Adegoke et al. (2003) demonstrated that intensive irrigation in Nebraska, USA, caused cooler surface temperatures and increased the latent heat flux. DeAngelis et al. (2010) detected a 15–30% increase in precipitation extending from the easternmost part of the Ogallala Aquifer to as far downwind as Indiana because of rapid increases in irrigation over the aquifer. Numerous studies using hydrological models have evaluated the effects of anthropogenic activities on land water resources. Although these models consider the processes of anthropogenic water exploitation, they usually emphasize the hydrological processes on the land surface and simplify other processes including energy and biophysical processes. The lack of energy processes makes it difficult to investigate the responses of the surface temperature or heat fluxes.

Land surface models (LSMs) include more detailed descriptions of land processes, and have advantages when investigating the influence mechanisms of water exploitation and consumption. Ozdogan et al. (2010) integrated satellite-derived irrigation data and high-resolution crop-type information into a land surface model to investigate the effects of irrigation on the land surface. They found that a 12% increase in evapotranspiration was caused by irrigation, with an equivalent reduction in sensible heat flux during the growing season of 2003. They assumed that the irrigation water was freely available for irrigation, but reservoirs or groundwater components were not included in the land surface model. There other modes of water consumption exist as wells as irrigation, including industrial and domestic uses. These types of consumption each constitute a certain proportion of the total water demand and should not be neglected when discussing the effects of water consumption. Furthermore, because water consumption is closely linked to the ways in which water resources are exploited, it should be an integral part of any model. Pokhrel et al. (2012) incorporated a water regulation module into the land surface model, MATSIRO in which the processes of human water withdrawal and consumption were considered. However, the LSM used in that study regarded groundwater as an isolated component, with no interactions with the soil layers. Groundwater storage was also treated as unlimited.

Despite numerous advances in modeling anthropogenic water withdrawal and consumption using LSMs, many improvements are still required. The aim of this study was to investigate the effects of groundwater exploitation on land surface processes (including both hydrological and energy processes) and the responses of land surface to different water demands. This study adds a conceptual scheme to LSMs, insofar as interactions between the soil layers and aquifers are included. The model used in this study also considers the depletion of groundwater by integral human water consumption. The Haihe River Basin, where the groundwater is severely overexploited, was chosen as the study domain. A series of historic and future simulations were conducted to identify the possible responses of land surface processes to groundwater exploitation. The following sections introduce some background information about the study domain and the model used, followed by descriptions of the scheme developed to model groundwater exploitation and the experimental design. The simulated results are then presented, including the historic and future simulations. Finally, we present a discussion and our conclusions.

2. Study domain

The Haihe River Basin in northern China covers an area of 318,200 km^2 (Fig. 1). Plateaus and mountains in the west and north account for 60% of the total area; the plains, where most of the inhabitants live, are the main agricultural areas and account for 40% of the total area. The Haihe River Basin is one of the most important agricultural areas in China and supports rapidly developing industries. Because of the low precipitation and high water demand there, the surface water resource cannot cope with the total water demand and an increasing volume of groundwater is being used, especially on the plains (Fei et al., 2006; Liu et al., 2008; Chen et al., 2010). In 2005, the volumes supplied were 8765 Mm^3 of surface water and 25,301 Mm^3 of groundwater in the Haihe River Basin. Hebei Province, which accounts for 54% of the total area of the Basin and contains most of the plain areas, consumes most of the groundwater supply in the Basin (16,068 Mm^3), and the volume of its surface water supply is only 3678 Mm^3 (Ren, 2007).

Since the groundwater is overexploited, local land water resources are declining rapidly, and an extreme water crisis has emerged in the Basin (Xu et al., 2004; Yang and Tian, 2009; Liang et al., 2011; Jia et al., 2012). Rivers at least 4000 km long, which account for about 40% of the total length of all rivers in the Basin, have become seasonal rivers. Wetland areas in the Basin have decreased by up to 90% since the beginning of the 1950s (Xia and Zhang, 2008). The overexploitation of groundwater, loss of water and soil, ecosystem degradation, and other eco-environmental issues threaten sustainable development in this region.

3. Model development and experimental design

3.1. Community Land Model (CLM3.5)

The Community Land Model (CLM) is a land surface model developed by the National Center of Atmospheric Research (NCAR) as part of the Community Climate System Model (Collins et al., 2006). CLM version 3.5 (Oleson et al., 2008) uses a tile approach to describe the heterogeneity of the land surface. Each grid cell contains four land cover types (glacier, wetland, lake, and vegetation), and the vegetated fraction can be further divided to 17 different plant functional types. It contains five possible snow layers and 10 soil layers.

CLM3.5 is a one-dimensional model that has fixed parameters on a global scale. Its hydrological processes are based on the SIMTOP model developed by Niu et al. (2005), and its groundwater component is in the form of an unconfined aquifer below the soil layers (Niu et al., 2007). The aquifer is treated as a simple homogeneous bucket, and the calculation of groundwater relies on the position of the groundwater table z_{∇} (m), which can be within the soil layers or below them. Water storage, W_t or W_a (mm), is calculated as:

$$\frac{dW_t}{dt} = q_{recharge} - q_{drai} \quad (z_{\nabla} < z_{h,10}), \tag{1}$$

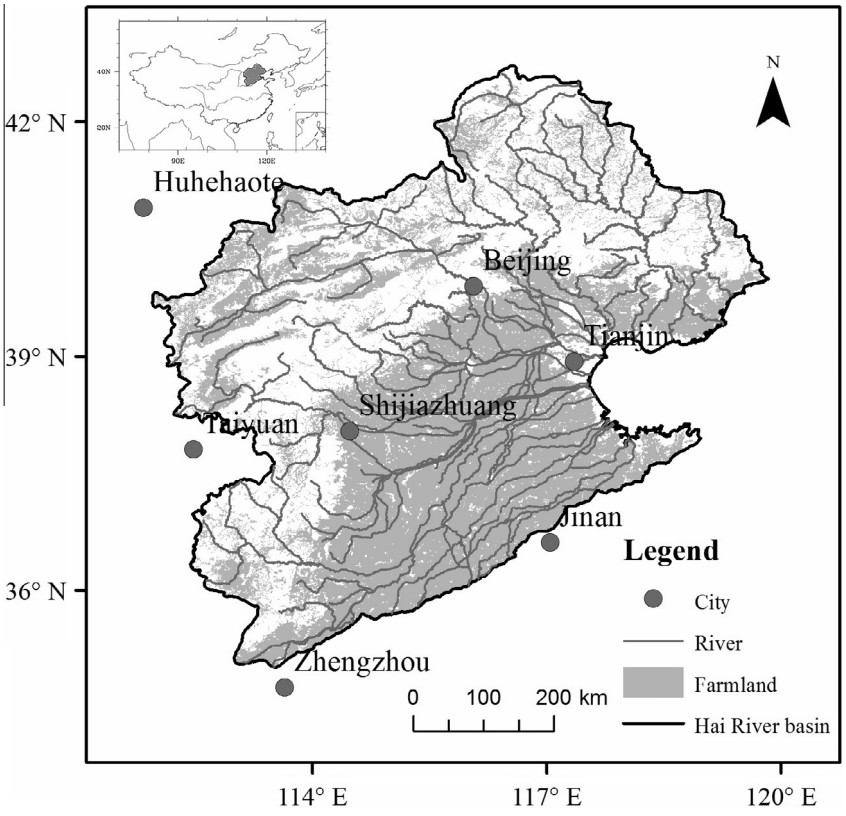

Fig. 1. Map of the Haihe River Basin and its location in China.

$$\frac{dW_a}{dt} = q_{recharge} - q_{drai} \quad (z_\nabla \geq z_{h,10}), \tag{2}$$

where $z_{h,10}$ is the depth of the 10th soil layer (m); $q_{recharge}$ is the groundwater recharge (mm/s); and q_{drai} is the groundwater outflow (mm/s). The groundwater recharge ($q_{recharge}$) is described as:

$$q_{recharge} = -k_a \frac{-10^3 z_\nabla - \left(\psi_{10} - 10^3 z_{10}\right)}{10^3 (z_\nabla - z_{10})}, \tag{3}$$

where k_a is the hydraulic conductivity of the aquifer (mm/s); ψ_{10} is the metric potential of the 10th soil layer (mm); and z_{10} is the depth of the midpoint of the 10th soil layer (m). Due to its structural limitations, CLM3.5 can only simulate the vertical water flow in a grid column; the lateral groundwater flow and the interactions of the groundwater among grid cells are not included in the model.

The calculation of soil temperature is based on the energy balance and the first law of heat conduction. The heat flux into the snow/soil surface from the atmosphere (h) is defined as:

$$h = S_g - L_g - H_g - \lambda E_g, \tag{4}$$

where S_g is the solar radiation absorbed by the ground (W/m^2); L_g is the long-wave radiation absorbed by the ground (positive when upward to the atmosphere) (W/m^2); H_g is the sensible heat flux from the ground (W/m^2); and λE_g is the latent heat flux from the ground (W/m^2). The heat flux from the soil bottom is set at zero. The energy balance for the ith soil layer is:

$$\frac{c_i \Delta z_i}{\Delta t}\left(T_i^{n+1} - T_i^n\right) = -F_{i-1} + F_i, \tag{5}$$

where i is the index of the soil layer; c_i is the heat capacity of the ith layer (J/m^3/K); Δz_i is its thickness (m); the values with superscript n and $n+1$ represent the first and last time steps; Δt is the time step (s); and F_{i-1} and F_i are the heat fluxes into and out of the ith layer (W/m^2), respectively.

Evapotranspiration in CLM3.5 is divided into the water flux from the ground (E_g) and the flux from the vegetation (E_v). They can be expressed by:

$$E_v = -\rho_{atm} \frac{(q_s - q_{sat}^{T_v})}{\gamma_{total}}, \tag{6}$$

$$E_g = -\rho_{atm} \frac{(q_s - q_g)}{\gamma'_{aw}}, \tag{7}$$

where ρ_{atm} is the density of atmospheric air (kg/m^3); q_s is the surface specific humidity (kg/kg); $q_{sat}^{T_v}$ is the saturation water vapor specific humidity at the vegetation temperature (kg/kg); γ_{total} is the total resistance to water vapor transfer from the canopy to the canopy air and includes contributions from the leaf boundary layer and sunlit and shaded stomatal resistances (s/m); q_g is the specific humidity at the ground surface (kg/kg); and γ'_{aw} is the aerodynamic resistance to water vapor transfer between the ground and the canopy air (s/m).

More detailed information about the physical parameterizations of the CLM is provided by Oleson et al. (2004). The CLM performs well in simulating the Earth's terrestrial water and energy cycles, which is why we chose to use it in this study (Tian et al., 2008; Sakaguchi and Zeng, 2009; Wang and Zeng, 2011; Huang et al., 2013).

3.2. Scheme for groundwater exploitation and its implementation in CLM3.5

A simple conceptual scheme describing the anthropogenic water consumption process was developed in this study (Fig. 2). In this scheme, for each time step, a specific quantity of water is

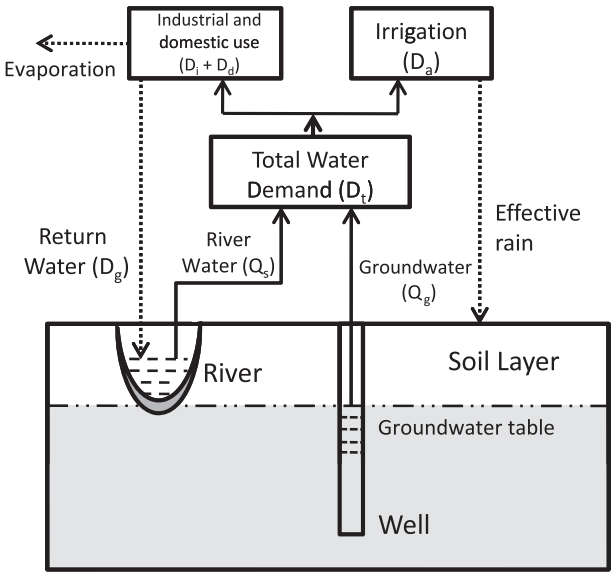

Fig. 2. Framework of the simulated human-induced water resource exploitation and utilization processes.

withdrawn from rivers and aquifers to meet the total water demand, D_t (mm/s). The stream flow quantity and groundwater quantity supplied are designated Q_s and Q_g (mm/s), respectively. The water withdrawn from rivers and from underground is consumed to meet the demands of three sectors: domestic demand D_d, industrial demand D_i, and irrigation demand D_a (mm/s). The water allocation to the industrial and domestic sectors is greatly simplified as being consumed by evaporation through various dissipation processes and as the wastewater returning to rivers (D_g) (mm/s). Unlike the water allocated to industrial and domestic use, all the water allocated to irrigation water consumption, D_a, is added to the effective rainfall that reaches the top of the soil layers. The increased effective rain will lead to further changes in other components (e.g., evapotranspiration, infiltration, etc.).

This scheme was incorporated into CLM3.5. For the exploitation process, the quantity of groundwater supplied, Q_g (mm/s), is subtracted from the groundwater storage. In this way, Q_g is taken into account during the calculation of the groundwater resource in CLM3.5:

$$\frac{dW}{dt} = q_{recharge} - q_{drai} - Q_g, \tag{8}$$

where $q_{recharge}$ is the groundwater recharge; q_{drai} is the subsurface runoff; and W is the groundwater storage W_t or W_a (mm). The supplied stream flow quantity Q_s (mm/s) is subtracted from the stream flow. In this way, the stream flow quantity in rivers, Q_r (mm/s), is expressed as:

$$Q_r = R_t + R_{str} - Q_s + D_g, \tag{9}$$

where R_t is the total local runoff which is the sum of surface runoff and subsurface runoff generated in the grid; R_{str} is the routed flow from upstream; and D_g is the wastewater discharge into rivers.

For the consumption process, the wastewater returning to the rivers after industrial and domestic consumption, D_g, is defined as $\alpha(D_i + D_d)$. The coefficient "α" is defined as the proportion of wastewater returning to rivers. The wastewater is treated as flowing into rivers outside the model column; the evaporation in the model increases by $(1-\alpha)\times(D_i + D_d)$ as a result of industrial and domestic consumption, and the effective rain also increases by D_a as a result of agricultural irrigation.

3.3. Estimation of water supply and demand

The process of groundwater exploitation is based on the assumption that the natural water resource can meet the total water demand in the basin. It will stop immediately when the groundwater table reaches bedrock. The depth of the bedrock is set at 80 m, which is the maximum possible depth of the groundwater table in CLM3.5. The balance between the water supply and demand is described as:

$$D_t = Q_g + Q_s. \tag{10}$$

The quantity of stream flow supplied, Q_s, in each grid cell is withdrawn from the local runoff generated R_t, and stream flow into the grid cell R_{str}. The stream flow is provided by the river routing model in CLM3.5 with a fixed spatial resolution $0.5^\circ \times 0.5^\circ$. In addition, to maintain the ecological base flow of the streams, exploitation of the stream flow is set not to exceed 80% of the total flow. Because stream flow is more conveniently exploited, the stream flow removal process is assumed to occur before the groundwater is pumped, with the latter taking place only if the local stream flow in the relevant grid cell is exhausted. Therefore, Q_s can be described as:

$$Q_s = \min(0.8 \times (R_t + R_{str}), D_t). \tag{11}$$

The quantity of groundwater supplied, Q_g, can be expressed by:

$$Q_g = \max(0, D_t - Q_s). \tag{12}$$

The total water demand D_t in each grid cell is estimated using relevant socioeconomic data, and can be expressed by:

$$D_t = D_d + D_i + D_a = \gamma_1 A_{pop} + \beta\gamma_2 A_{GDP} + \gamma_3 A_{agr}, \tag{13}$$

where γ_1 is the average domestic water consumption per capita; A_{pop} is the population in each grid cell (capita); β is an empirical conversion ratio for the gross domestic product (GDP) and the value of the industrial output; γ_2 is the average industrial water consumption per 10,000 yuan of industrial output; A_{GDP} is the GDP (yuan); γ_3 is the average consumption of irrigation water per unit area of cropland; and A_{agr} is the area of irrigated land (km^2).

In this study, the social datasets (for population and GDP) are those for 2000 A.D. based on the Department of Urban and Social Economic Survey, National Bureau of Statistics of China (2001), which were processed at a resolution of 1 km × 1 km by the Data Center for Resources and Environmental Sciences, Chinese Academy of Sciences. The farm area dataset is derived from the Scientific Data Center in Cold and Arid Regions, Chinese Academy of Sciences (Ran et al., 2012). These socioeconomic datasets are summed at a 0.25° grid resolution to estimate the water demand. The average water consumption data (γ_1, γ_2, γ_3) are from the *China Water Resource Bulletin 2000*. As shown in Table 1, the estimated water demands by Eq. (13) basically correspond to the actual values for the Haihe River Basin in 2000. Fig. 3a shows the spatial distribution of the water demand. The plains in the east and south of the Basin account for a large proportion of the total population and represent a major part of the water demand. The mountainous regions demand less water because their populations are sparser. The cities on the plain, including Beijing, Tianjin, and Shijiazhuang, consume more water per unit area than other rural regions, to meet the demands of their high populations and dense industrial establishments. The statistics for the total water demand in the Basin from 1965 to 2000 were derived from Wei et al. (2006) and the *Water Resource Bulletin of Haihe Basin*. These figures were not available for every year in that period, and the missing values in the early years were derived by linear extrapolation. Using these statistical values, the estimated water demands in 2000 A.D. were scaled down, keeping the proportions for the three water-consuming sectors unchanged, to approximately represent the changes in

Table 1
Estimated water demands and actual statistical values in 2000.

	Industrial use (Mm^3)	Domestic use (Mm^3)	Agricultural use (Mm^3)	Total quantity (Mm^3)
Estimated	8060	5080	35,720	48,860
Actual	6570	5180	28,090	39,840

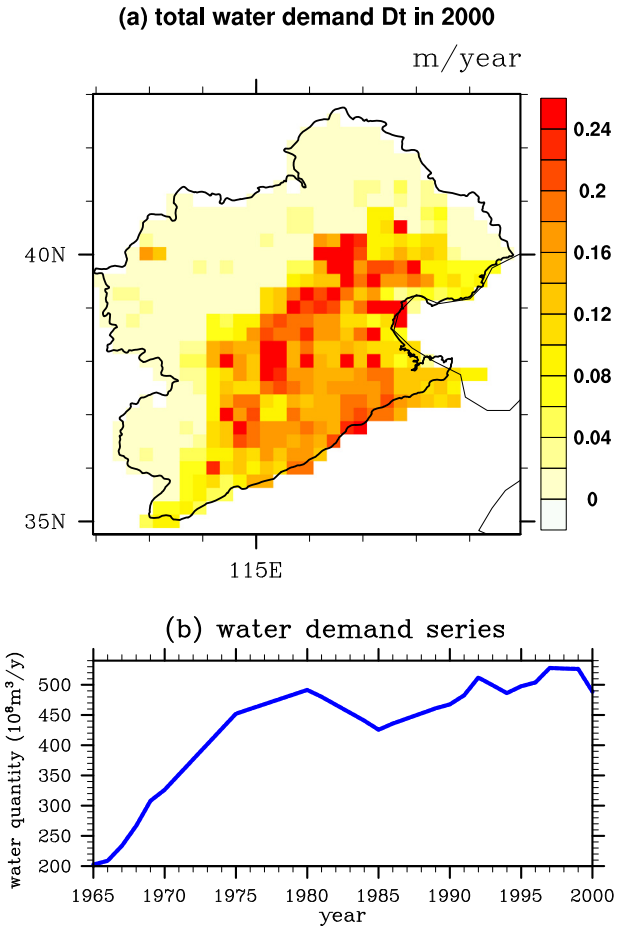

Fig. 3. (a) Spatial distribution of the estimated water demands in 2000 for the Basin; and (b) the series of estimated water demands from 1965 to 2000.

water demand during the simulation period. As shown in Fig. 3b, the estimated water demand in the Basin increased rapidly before 1980, but did not change greatly thereafter because water-use efficiency improved as the economy developed.

The water quantity for each sector of the scheme was obtained by estimating the water supply and demand. The proportion of the wastewater in the industrial and domestic consumption that returned to the rivers, α, was arbitrarily set at 30% based on data from Mao et al. (2000). In regions with scarce water resources, wastewater is partly used for urban landscaping and other facilities, and does not return to the rivers all. The proportion α does not represent the primary proportion of the wastewater generated in factories but instead is an estimate of the proportion of wastewater discharge flowing downstream. The actual proportion may be even less than 30%. According to the *Water Resource Bulletin of Haihe Basin*, the river recharge to the sea in 2000 was only 410 Mm^3, far less than the total water demand of 39,840 Mm^3. This discrepancy indicates that nearly all the water resource is dissipated in the Basin and does not flow into the sea as wastewater discharge.

3.4. Experimental design

Four historic simulation experiments were conducted for the years 1965–2000 under different water demands, three hypothetical experiments for the years 2001–2200, and three experiments for the years 2001–2100 with future climate scenario. Table 2 lists the settings used in these experiments. In these simulations, we used the land surface model CLM 3.5 with the implemented groundwater exploitation scheme. This study focuses on the climatological changes of variables. All the changes are multi-year mean values or annual values. Therefore, the annual irrigation water was applied equally throughout the year and seasonal variations in the irrigation demand were not considered. The model domain was set at 105°–127°E, 30–46°N, and was centered on the Haihe River Basin, and the resolution was $0.25° \times 0.25°$. Princeton global three-hourly atmospheric data at a spatial resolution of $1° \times 1°$ were used as the forcing atmospheric data for the model (Sheffield et al., 2006). The forcing data were then downscaled to match the simulation resolution during the preprocessing step using the internal interpolation function in CLM3.5.

The historical simulation experiments for years 1965–2000 (P1, P2, P3, CTL) were performed first to determine the effects of groundwater exploitation on land processes and to investigate the sensitivity of the effects caused by different water demands. Using the water demands estimated in Section 3.3, one simulation test (P1) was performed for the water demand in 2000 and another (P2) for the water demand in 1965. The water demands of these two tests remained constant throughout the 36-year simulation period. A third simulation test (P3) was performed for the varying demand from 1965 to 2000, and the control test (CTL) was also used to simulate the natural state, ignoring human-induced perturbations. Before commencing the simulation, a spin-up of 100 years, driven by the historical climate data for 1955–1964, was repeated 10 times to obtain balanced groundwater conditions so that the historical simulations had the same initial states. The groundwater depth and soil moisture after the spin-up (Fig. 4) correlated well with the local climatology. The northwestern desert and grassland regions in the figures have drier soils and deeper groundwater, whereas the humid regions in the southeast have soils with a higher moisture content and the water table is closer to the land surface.

Another group of hypothetical simulations based on the final P3 result in 2000 was conducted, running forward for 200 years. One simulation (Pmp) continued the exploitation process of P3, using the water demand in 2000 in such a way that groundwater exploitation would stop if the local water table fell to bedrock. Another simulation (Rst) was also based on the results of P3 in 2000, but with no further water demand, that is, the process of water utilization and groundwater exploitation was simulated to cease completely to restore the groundwater. The control simulation (termed "CTL_E" to distinguish it from the previous CTL test) was also run for 200 years. The three simulations were driven by one-year climatic data that were averaged by the historic data from 1991 to 2000. Thus, the climatic forcing data had no interannual variation, and changes in the variables were based solely on the responses of the land surface conditions, ignoring changes in climate.

Climate projections for the future were taken into account in three additional simulations projected for 100 years, for comparison with the hypothetical simulations that did not include climate changes. These simulations were also based on the final results of P3 in 2000 and are designated Pmp_F, Rst_F, and CTL_EF. These three simulations were similar to the previous ones (Pmp, Rst, and CTL_E, respectively), but they were driven by the output of the general circulation model (GCM) of the RCP4.5 experiment of

Table 2
Settings of the conducted simulation tests.

Name	Time period	Initial condition	Water demand	Climate forcing
P1	1965–2000	1964, after spin-up	2000, constant	Princeton (1965–2000)
P2	1965–2000	Same as P1	1965, constant	Same as P1
P3	1965–2000	Same as P1	1965–2000	Same as P1
CTL	1965–2000	Same as P1	None	Same as P1
Pmp	2001–2200	P3 in 2000	Same as P1	Annual data averaged from Princeton (1991–2000)
Rst	2001–2200	Same as Pmp	None	Same as Pmp
CTL_E	2001–2200	CTL in 2000	None	Same as Pmp
Pmp_F	2001–2100	Same as Pmp	Same as P1	Princeton (2001–2005) + FGOALS (2006–2100)
Rst_F	2001–2100	Same as Pmp	None	Same as Pmp_F
CTL_EF	2001–2100	Same as CTL_E	None	Same as Pmp_F

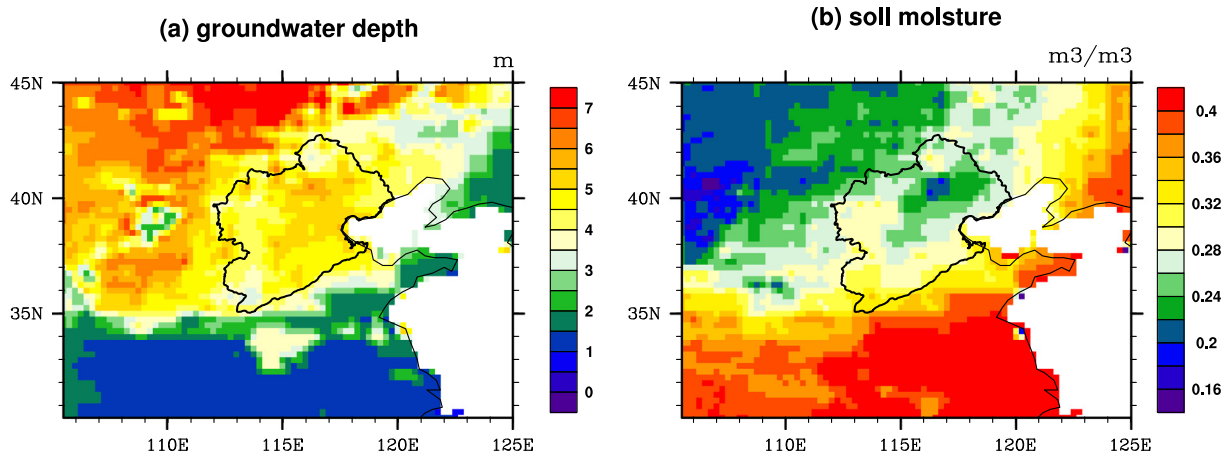

Fig. 4. Spatial distribution of (a) groundwater depth after spin-up; and (b) total soil moisture after spin-up.

the Coupled Model Intercomparison Project Phase 5 (CMIP5) (Taylor et al., 2012). The RCP4.5 scenario was chosen in this study because its emission is designed as a middle scenario with medium CO_2 emission in the future. The GCM output data were derived from the simulation of version g2 of the Flexible Global Ocean Atmosphere Land System (FGOALS-g2) developed at the State Key Laboratory of Numerical Modeling for Atmospheric Sciences and Geophysical Fluid Dynamics of the Institute of Atmospheric Physics, Chinese Academy of Sciences. The output data from RCP4.5 were only available for 2006–2100. The forcing data for 2001–2005 were derived from the Princeton historical climate data.

4. Results

4.1. Validation of the simulation tests

The validations of four variables (groundwater table, soil moisture at 10 cm depth, total runoff, and terrestrial water storage change) simulated with CLM3.5 are provided here. Fig. 5 shows the spatial distributions of the observed and simulated groundwater table for 2000. The monthly groundwater table observations for 2000 were provided by the Ministry of Water Resource and Institute for Geo-Environmental Monitoring in China, and the values in the grid cells without observations were set as missing

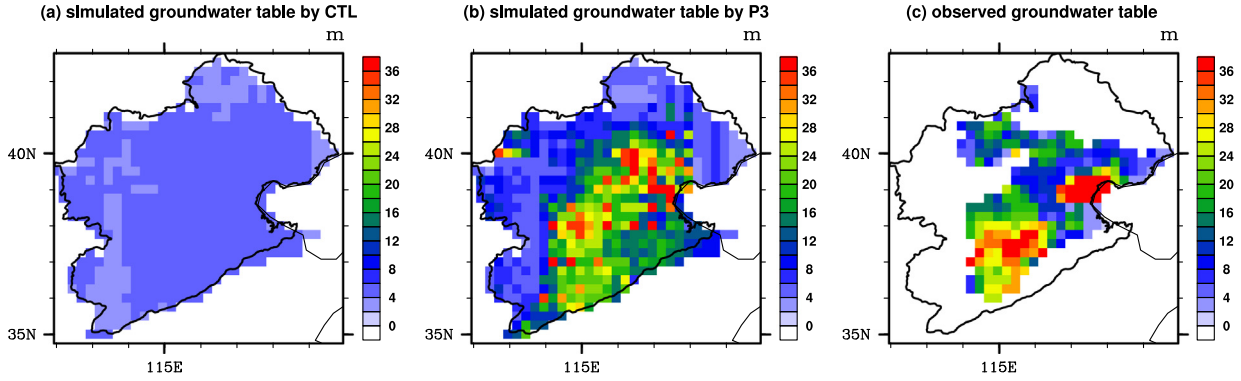

Fig. 5. Spatial distribution of (a) simulated groundwater depth in 2000 on the control test; (b) simulated groundwater depth in 2000 on the P3 test; and (c) observed groundwater depth in 2000.

values. As seen in Fig. 5a, the groundwater table simulated with the control test was generally at a depth of 3–6 m in the Basin, and was slightly deeper in the plains than in the western and northern mountains. The observed groundwater table (Fig. 5c) was far deeper than the results produced with the control simulation. It exceeded 6 m in most plain areas, and in some areas near Shijiazhuang (114.5°E, 38°N) and Tianjin (117°E, 39°N), the water table even exceeded 30 m. Although P3 simulated the rapid decline in the groundwater table (Figs. 5b and 6a), the spatial distribution of the simulated groundwater differed greatly from the observed distribution, and the simulated depth to the water table was higher than the observed depth. The difference between P3 and the observed results was probably related to the lack of lateral flow of the groundwater and the fixed specific yield of the aquifers in CLM3.5. Also, the overestimated water demands led to the higher simulated water table. Generally, increased evaporation would enhance the local atmospheric convective activities and increase the probability of convective rainfall. Since the observational data are coarsely distributed and sparse, the spatial distributions of the related variables are not presented. Fig. 6 shows the time series of the groundwater table, 10 cm soil moisture, and seasonal changes of total runoff, and terrestrial water storage. Observed groundwater table data were available from 1991 to 2000 (Fig. 6a). Accordingly, the simulated groundwater table was averaged over the grid cells for which the observations were available. The groundwater simulated with the control test did not change greatly during this period of time. In comparison, the groundwater table simulated with the P3 test was deeper and declined more rapidly than it did in the control test or in the observed data. Fig. 6b shows the 10 cm soil moisture data. The observed data from 1993 to 2000 were derived from the China Meteorological Data Sharing Service System (available in Chinese at http://cdc.cma.gov.cn/), and the simulated results were averaged in the grid cells using the available observations. The simulated 10 cm soil moisture was on average wetter (by about 0.05 m^3/m^3) and showed less seasonal variation across the months of a year than the observed data. Fig. 6c shows the multiyear mean monthly runoff. The observation data are from the Global Runoff Data Center (www.bafg.de/GRDC) and are multiyear average data with no interannual variations. For comparison, the average runoff simulated by CLM3.5 from 1965 to 2000 is provided. Because the upper soil was wetter and the groundwater table shallower in CLM3.5, the simulated runoff generated in the Basin was about 7 mm/year more than the observed runoff, and it displayed less seasonal variations. The multiyear mean changes in terrestrial water storage are shown in Fig. 6d. The observation data are from the Gravity Recovery and Climate Experiment (GRACE) (Tapley et al., 2004) and were available for 2003–2012. The simulated changes in terrestrial water storage were averaged from 1965 to 2000. Despite the mismatch in the time period, the multiyear mean values still reflected the seasonal variations in terrestrial water storage in some respects. The simulated changes in terrestrial water storage were calculated from the total precipitation (*Pre*) minus the sum of evapotranspiration (*ET*) and total runoff (R_t). As shown in Fig. 6d, the simulated changes in terrestrial water storage were usually higher than the GRACE data in spring and summer. The greatest differences were 60 mm, occurring in July. The P3 test simulated a greater reduction in terrestrial water storage than the control test, but this difference was smaller than the difference between the simulations and the observation data.

The annual water supply volumes in the Haihe Basin from 1997 to 2000, accounted for 62.7%, 72.5%, 62.6%, and 70.0%, respectively. During the period, the actual groundwater resource supply, derived from the *Water Resource Bulletin of Haihe Basin* and the *Chinese Water Resource Bulletin of Haihe Basin*, accounted for 60.8%, 61.8%, 67.6%, and 65.6%, respectively. The proportion of simulated groundwater supply was slightly larger because the surface water in the CLM model could only be pumped from rivers. The lack of reservoirs, lakes, and water diversions from the outer Basin in the model leads to greater groundwater exploitation.

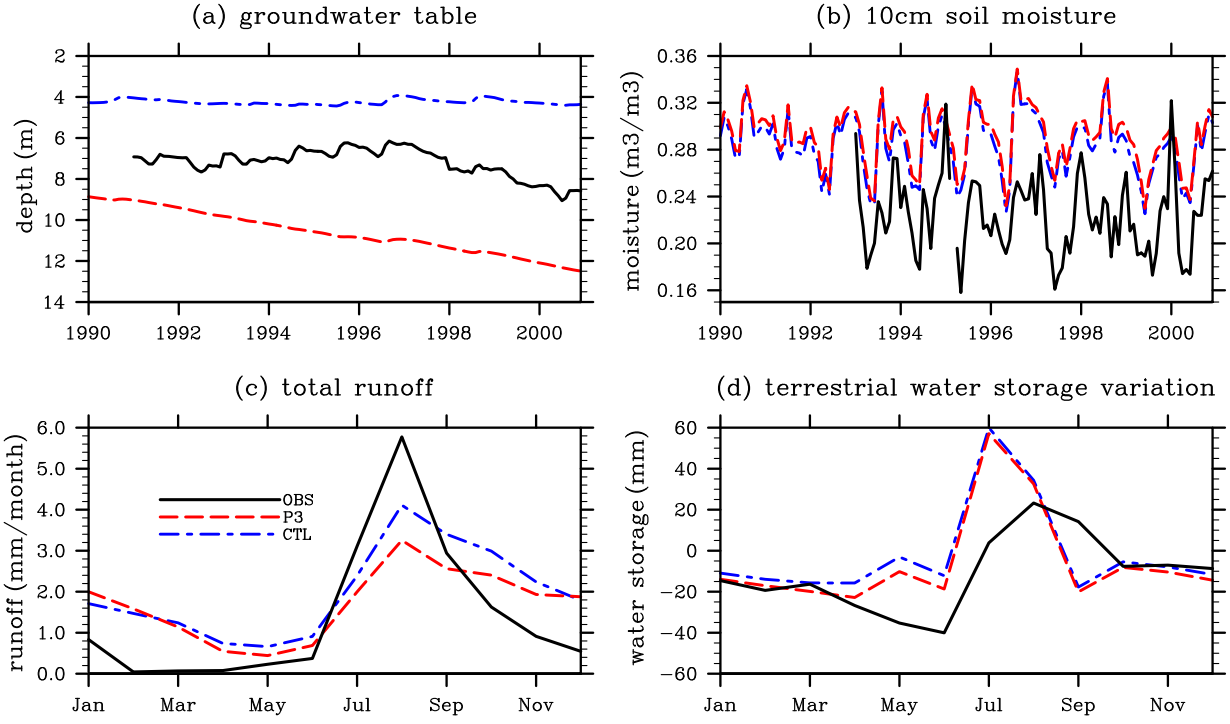

Fig. 6. (a) Monthly series of the groundwater table; (b) monthly series of 10 cm soil moisture; (c) multiyear mean monthly total runoff; and (d) multiyear mean monthly changes in terrestrial water storage in the P3 test, control test, and observational data.

4.2. Effects of groundwater exploitation on land surface processes

4.2.1. Spatial distribution of differences

In the historic simulations, the land surface conditions in the Basin, including the groundwater, soil, heat flux, etc., changed greatly in response to groundwater exploitation over the 36-year simulation period. Fig. 7 shows the spatial distributions of the groundwater table and soil moisture by the end of the simulation period. A funnel-shaped groundwater table appeared in the southern plains of the Basin after exploitation for 36 years. As seen in Fig. 7a–c, the water table fell greatly on the plains, where most of the cities are located. In some areas with a large water demand (e.g., Shijiazhuang [114.5°E, 38°N], Tianjin [117°E, 39°N], Beijing [116.5°E, 40°N], and their surrounding regions), the water table fell to more than 20 m below the ground surface (Fig. 7a and c). However, in the western and northern mountainous areas of the Basin, it fell only slightly because the economy is less developed and the population sparse. The falling level of the groundwater table in the three simulations was closely related to the different water demands. The areas shaded by strips in the spatial distribution figures indicate that the changes were statistically significant, with a confidence level of 95%. As more water was withdrawn from the groundwater for irrigation, the upper soil became wetter because more water reached the topsoil. However, the rapidly falling groundwater table in the three exploitation tests caused the soil layers to become hydraulically disconnected from the groundwater table. With the increased depth of vadose zone, the rate of vadose from the bottom soil layer approached free gravitational drainage, k_a (hydraulic conductivity of the aquifer)—see Eq. (3). Therefore, the total soil moisture was affected by the wetter topsoil and the increased soil drainage into the aquifers, and the moisture changes in the soil layers depended on whether the increased infiltration from the topsoil could retard the drying of the lower soil layers. As seen in Fig. 7d–f, the total soil moisture in the three exploitation tests changed by about 0.0023 m^3/m^3, −0.0006 m^3/m^3, and 0.0019 m^3/m^3 on average in the Basin. Unlike in the other two tests, in the P2 test with a low water demand, the soil became drier almost across the entire Basin. Other than that, the changes in the total soil moisture in the three simulations were not significant in most areas, with the exception of a few mountainous and farmland areas.

A wetter upper soil also creates more surface runoff. As shown in Fig. 8a–c, average increases in surface runoff of about 1.47 mm/y, 0.31 mm/y, and 1.46 mm/y were detected with the three tests in 2000. A significantly greater difference in runoff was detected in the mountainous area northwest of the Basin, where there was an increase in total soil moisture. However, the differences in subsurface runoff in 2000 (Fig. 8d–f) were −0.16 mm/y, −0.27 mm/y, and −0.15 mm/y for the three tests. The differences were negative in most areas of the Basin in 2000, but this was not always true for the whole simulation period. The changes were also significant in some plain areas where the groundwater declined most markedly. The moisture at the land surface changes with human-induced disturbance of the land water resource, so does the land surface temperature. The differences in ground temperature (temperature at the land surface) in 2000 are shown in Fig. 8g–i. In the three simulations, cooling effects were detected on the surface of the soil layers. The reductions in ground temperature (0.27 K, 0.06 K, and 0.20 K) were positively related to the local water demand. The reduction in ground temperature was greatest in the regions of highest water demand in the plains, by more than 0.3 K in P1 and P3, and by more than 0.1 K in the P2 test. Apart from those, the changes in ground temperature were not significant. According to Pokhrel et al. (2012), the decline in the annual mean

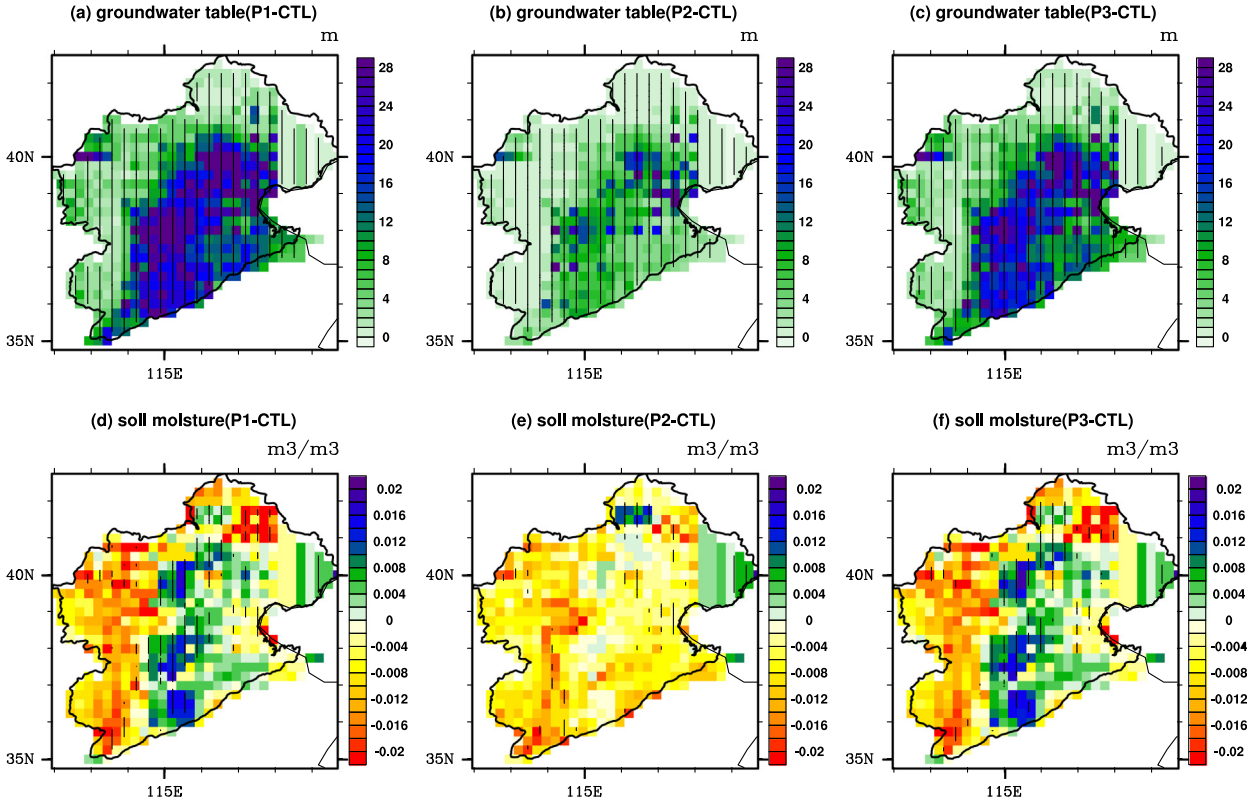

Fig. 7. Spatial distributions of (a) groundwater table differences (P1 – CTL) in 2000; (b) groundwater table differences (P2 – CTL) in 2000; (c) groundwater table differences (P3 – CTL) in 2000; (d) total soil moisture differences (P1 – CTL) in 2000; (e) total soil moisture differences (P2 – CTL) in 2000; and (f) total soil moisture differences (P3 – CTL) in 2000.

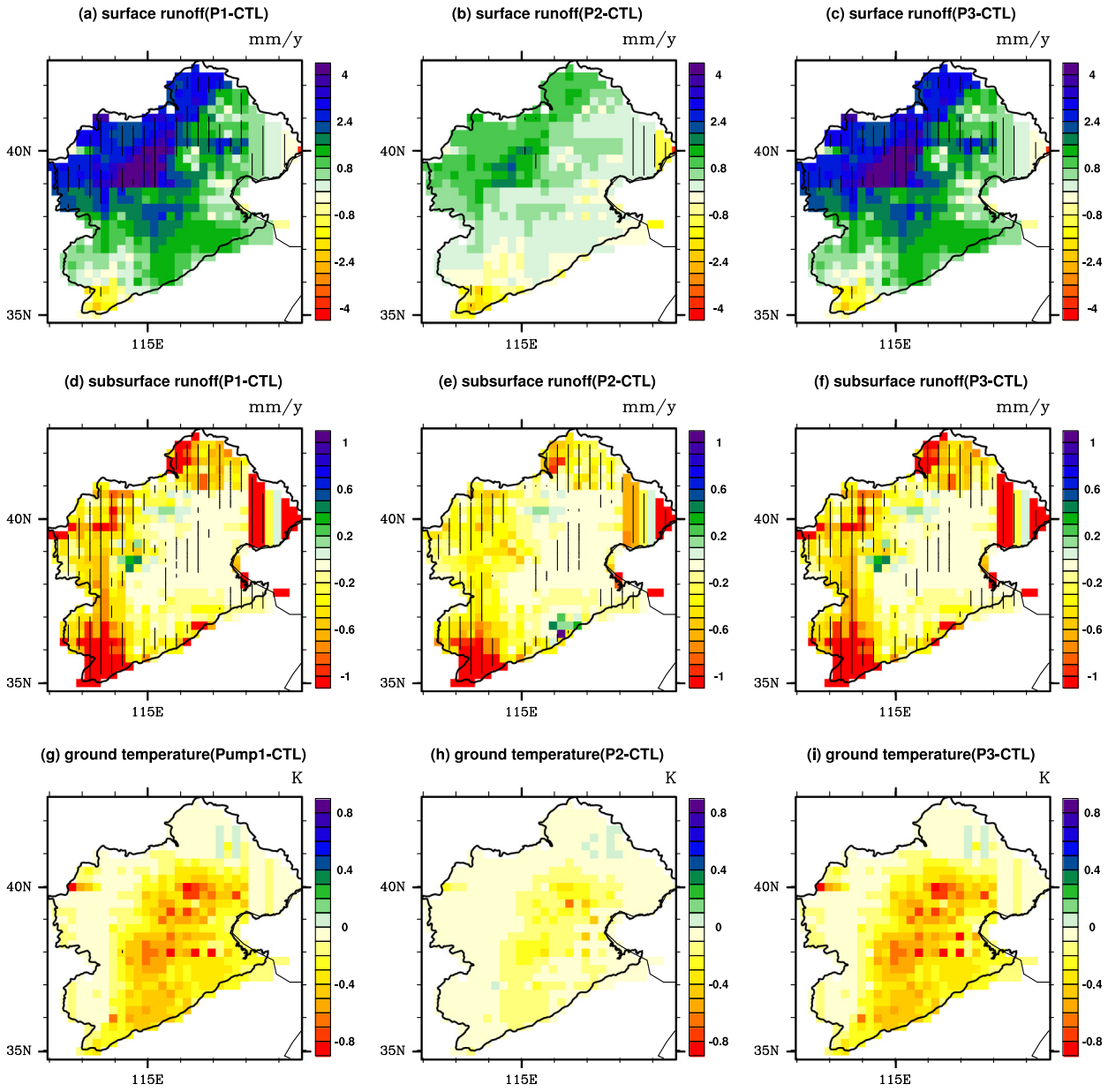

Fig. 8. Spatial distributions of (a) surface runoff differences (P1 – CTL) in 2000; (b) surface runoff differences (P2 – CTL) in 2000; (c) surface runoff differences (P3 – CTL) in 2000; (d) subsurface runoff differences (P1 – CTL) in 2000; (e) subsurface runoff differences (P2 – CTL) in 2000; (f) subsurface runoff differences (P3 – CTL) in 2000; (g) total soil temperature differences (P1 – CTL) in 2000; (h) total soil temperature differences (P2 – CTL) in 2000; and (i) total soil temperature differences (P3 – CTL) in 2000.

surface temperature is about 0.04 K when averaged across the grid cells on a global scale. The greatest decline in surface temperature is about 3.3 K in summer. The changes in the surface temperature did not differ greatly from the results of Pokhrel et al. (2012). The mean values for the reductions in temperature were slightly greater than the globally averaged values because of the high water demand in the Haihe River Basin. It follows from Eq. (4) that the increased evaporation caused by water consumption leads to a reduction in the heat flux entering the topsoil, and the soil temperature decreases in consequence. Although the lowering of the surface temperature causes a further reduction in sensible heat, the total heat flux released from the land surface in the three exploitation tests remained greater than that in the control test, and in this way, a cooling effect was apparent in the Basin.

The spatial distributions of the air temperature differences are shown in Fig. 9a–c. The 2 m air temperature in CLM3.5 is a diagnostic variable, which is determined from the surface temperature, surface roughness, and other parameters. The distribution of the 2 m air temperature was similar to that of the ground temperature, but the average reductions in temperature (0.11 K, 0.03 K, and 0.06 K) were less than those for the soil. In Fig. 9, a colder land surface led to reduced sensible heat fluxes in the water-pumping simulations, with corresponding increases in the latent heat fluxes. On average, reductions in the sensible heat flux of around 1.95 W/m^2, 0.60 W/m^2, and 2.17 W/m^2, and corresponding increases in the latent heat fluxes of around 4.10 W/m^2, 1.67 W/m^2, and 4.01 W/m^2, respectively, were detected in the Basin with the three tests after exploitation for 36 years. The most significant changes occurred on the plains, especially in areas close to cities where more water was consumed. According to Ozdogan et al. (2010), irrigation in the continental United Sates caused an increase of 9 W/m^2 in the latent heat flux and a reduction of 8 W/m^2 in the sensible heat flux during the crop-growing season in 2003. The results provided in this study are annual mean values and are slightly less than the averaged results for April to October.

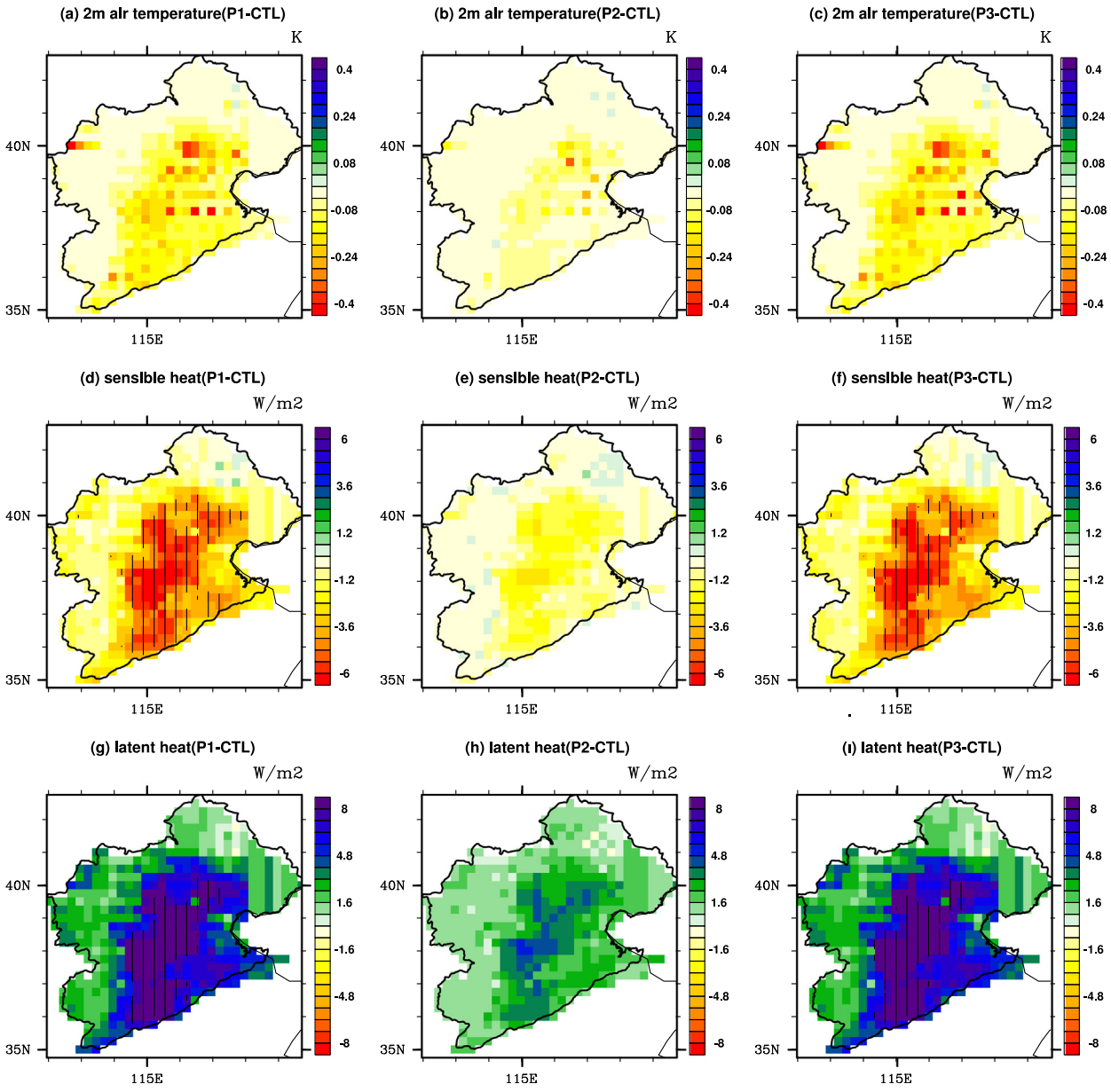

Fig. 9. Spatial distributions of (a) 2 m air temperature differences (P1 – CTL) in 2000; (b) 2 m air temperature differences (P2 – CTL) in 2000; (c) 2 m air temperature differences (P3 – CTL) in 2000; (d) sensible heat flux differences (P1 – CTL) in 2000; (e) sensible heat flux differences (P2 – CTL) in 2000; (f) sensible heat flux differences (P3 – CTL) in 2000; (g) latent heat flux differences (P1 – CTL) in 2000; (h) latent heat flux differences (P2 – CTL) in 2000; and (i) latent heat flux differences (P3 – CTL) in 2000.

4.2.2. Temporal variability and vertical soil profiles

The time series shown in Fig. 10 were analyzed using 12-month moving averages to remove seasonal variations. Fig. 10a shows the monthly series of basin-averaged differences in groundwater depth. The water table dropped continuously in the water-pumping simulations as water was taken from the aquifers to the land surface to meet human needs. The three tests showed similarly decreasing trends, but with different magnitudes because the intensities of groundwater exploitation differed. On average, the P1 and P3 tests, with greater water demands, showed the water table falling about 9–10 m more than the control test by the end of the simulation period. In contrast, the depth difference between P2 and the control test was about 4 m. In Fig. 10b of the soil moisture differences, increasing wetting trends were detected in the three exploitation tests compared with the control test. The high-intensity water consumption of the P1 test led to an increase in the amount of water infiltrating the soil, creating a positive soil moisture difference in most years. No soil layers in the P2 test were wetter than the control test because the lower irrigation usage was unable to balance the changes in the recharge from the soil layers to the aquifers. By comparison, the low-level water consumption in the P3 test made the soil moisture differences similar to those in the P2 test early in the simulation period. However, as the water demand increased, the P3 test performed increasingly and an obvious transition point was detected before the 1980s for many of the variables other than soil moisture, including surface runoff, sensible heat flux, etc.

The differences in surface and subsurface runoff are shown in Fig. 10c and d. The simulated surface runoff and subsurface runoff were clearly greater in the P1 test than in the control test. For the P2 test, the runoff differences were negative in most years, corresponding to drier soil layers. For the P3 test, its transition from the status of P2 to that of P1 was also detected in the period before 1980. The differences between the three tests and the

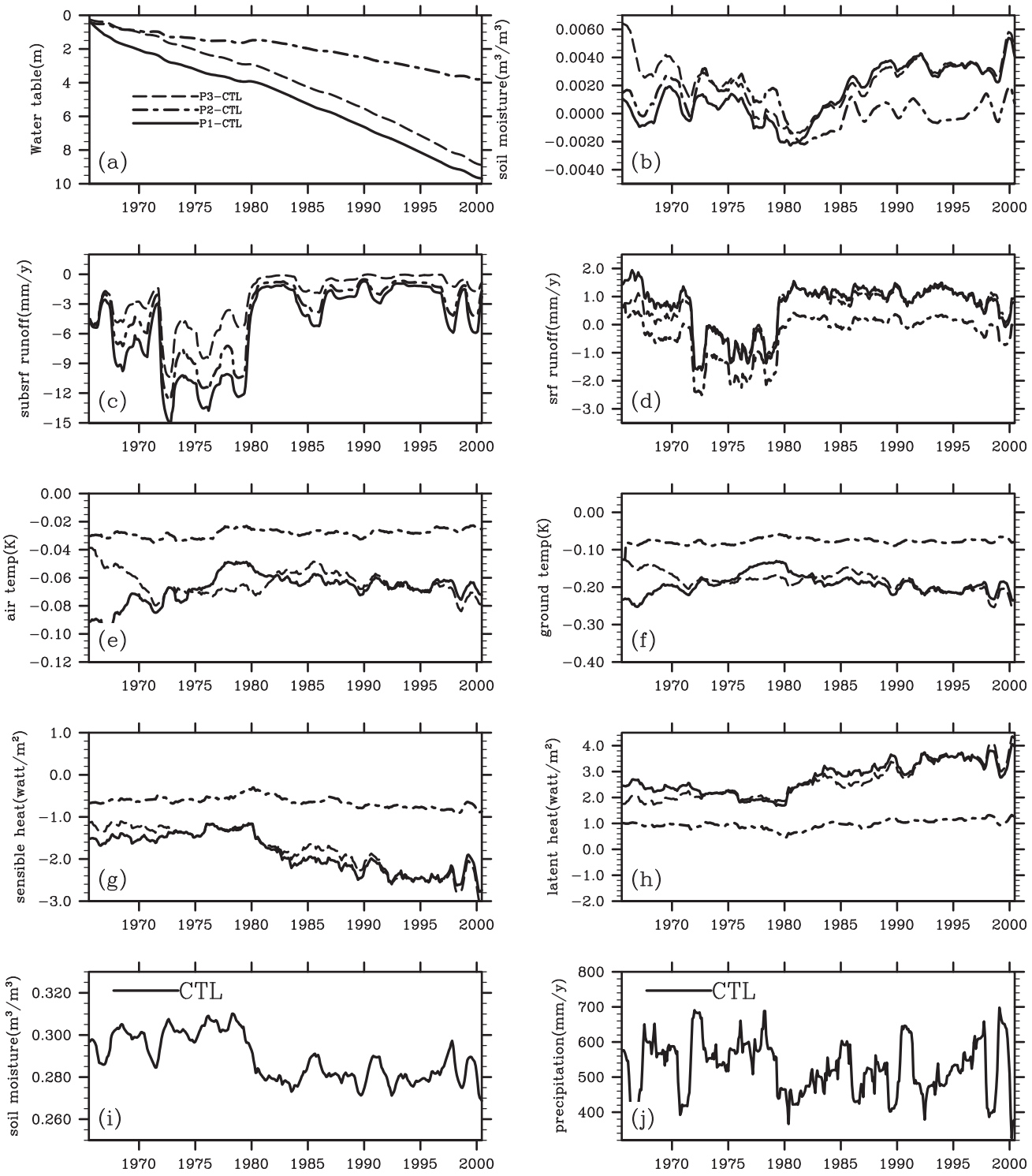

Fig. 10. Time series of basin-averaged (a) groundwater table differences; (b) total soil moisture differences; (c) subsurface runoff differences; (d) surface runoff differences; (e) 2 m air temperature differences; (f) total soil temperature differences; (g) sensible heat flux differences; (h) latent heat flux differences; (i) total soil moisture in the control tests; and (j) precipitation forcing.

control test showed slightly decreasing trends, probably attributable to the drying trend over the previous years, because the water consumption processes in the exploitation tests did not vary greatly. As seen in Fig. 10i and j, precipitation decreased greatly around 1980 and this low precipitation continued for about 15 years, until 1995. With reduced precipitation, there was an abrupt change in soil moisture around 1980. The declining trend in soil moisture made it less likely that any water that reached the soil surface would generate runoff, so that the usual increased runoff from irrigation decreased slightly over that period, especially in the P1 and P3 tests after 1980.

Fig. 10e and f shows the 2 m air temperature differences and ground temperature differences. The temperature differences showed slightly increasing trends, which indicated that the cooling effects were reinforced by water pumping. Unlike the other variables, the simulated temperature for the P3 test did not reach

the P1 test level and remained slightly higher throughout the simulation period. The decreasing differences in sensible heat flux and the increasing differences in latent heat flux, corresponding to the accumulating cooling effects, are shown in Fig. 10g and h. The total energy flux differences (sensible plus latent flux differences) remained positive for the three exploitation tests, indicating that the water consumption process led to a higher rate of energy emission from the land surface throughout the simulation period.

Fig. 11 shows the profiles for average soil moisture and temperature in 2000. For the three water-pumping simulations, the water used for irrigation caused the upper soil layers to become much wetter, whereas the lower layers became drier as the groundwater table fell rapidly and there was greater recharge into the aquifers. The differences in soil temperature showed little change in the vertical direction because in CLM3.5, the bottom soil layer is set to be thermally isolated from the aquifer below it, so that all the changes in soil temperature are attributable only to the changes in heat flux into the soil surface above. Thirty-six years of human exploitation of water has redistributed the land's water resources and caused a series of changes in moisture and energy amounts and fluxes. The moisture-related variables include wetter upper soil layers, increased surface runoff, a lowered groundwater table, and depleted land water storage. The changes in land surface moisture have also disturbed the energy balance, with increased evaporation reducing the land surface temperature and increasing the energy output compared with those in the natural state.

4.3. Responses of the land surface to different policies regarding groundwater exploitation

As discussed above, water exploitation over 36 years has changed the hydrological and thermal conditions of the land surface in the Haihe River Basin. However, land water resources are finite and slow to recover. In the Basin, where most areas are semiarid, it will not be possible to meet the current high water demand for long. How the moisture and energy conditions in the Basin will change in the future is of great concern. Therefore, we devised two hypothetical extreme future scenarios based on the results of the P3 test in 2000. The first outlined the likely consequences of continuing the present exploitation process unchanged (i.e., using the demand, D_t, measured in 2000; "Pmp" test and "Pmp_F" test); in the second scenario, all exploitation was stopped now to allow the water resources to recover ("Rst" test and "Rst_F" test). The exploitation process would be forced to stop in any case, when no more local water resources were available.

Fig. 12 shows the differences between the two hypothetical tests (Pmp and Rst test) and the control test (CTL_E) driven by constant climate forcing over 200 years. In Fig. 12a, the Pmp test, which continued the exploitation process at the water demand rate of 2000, showed that the land water storage would still decline quickly, but at a slower rate, as increasing numbers of grid cells suffered water resource depletion over time. However, the results of the second extreme scenario—the Rst test, in which all exploitation was stopped now to allow the water resources to recover—showed that the land water storage would be slowly restored to its natural condition. It is noteworthy that it did not return to its original state within 200 years; even more time was required to restore the local water resource. As shown in Fig. 12b, the total water deficiency was defined as the difference between the total water demand, D_t, and the actual groundwater quantity pumped per year. During the simulation period, for each time step, once the groundwater table began to drop to the bedrock depth in one grid cell, the water deficiency was calculated as the water demand (D_t) minus the total runoff (R_t). In Fig. 12b, the total water deficiency is the summed values in all the grid cells. By the end of 2000, a water deficiency of about 3 billion cubic meters per year was detected. At present, this deficiency can still be resolved, for example, by taking resources from nearby regions or reducing the allocation of water to inefficient facilities and factories. However, by 2200, the total water deficiency will increase to over 29 billion cubic meters per year, and it will be impossible to meet the original 2000 demand of 48.86 billion cubic meters per year. Most grid cells with a water deficit are in the plain areas, where the groundwater table dropped most rapidly. The spatial distribution of water deficiency (not shown) resembled those in Fig. 7a and c (i.e., the differences in the groundwater table).

The Pmp simulation indicated that the groundwater table (Fig. 12c) will have dropped about 40 m in 2200, by which time about one half of the Basin will suffer water deficiency. The groundwater depth in the Rst test rose only about 3 m after natural recovery for 200 years compared with the control test (CTL_E). This low rate of recovery is attributable not only to the slow changes in

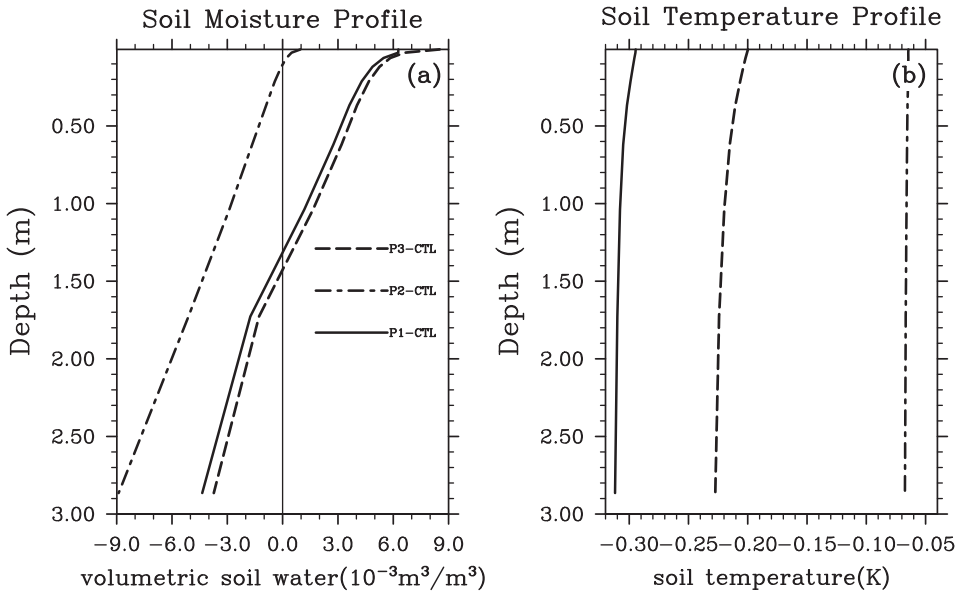

Fig. 11. Profiles of (a) soil moisture differences in 2000; and (b) soil temperature differences in 2000.

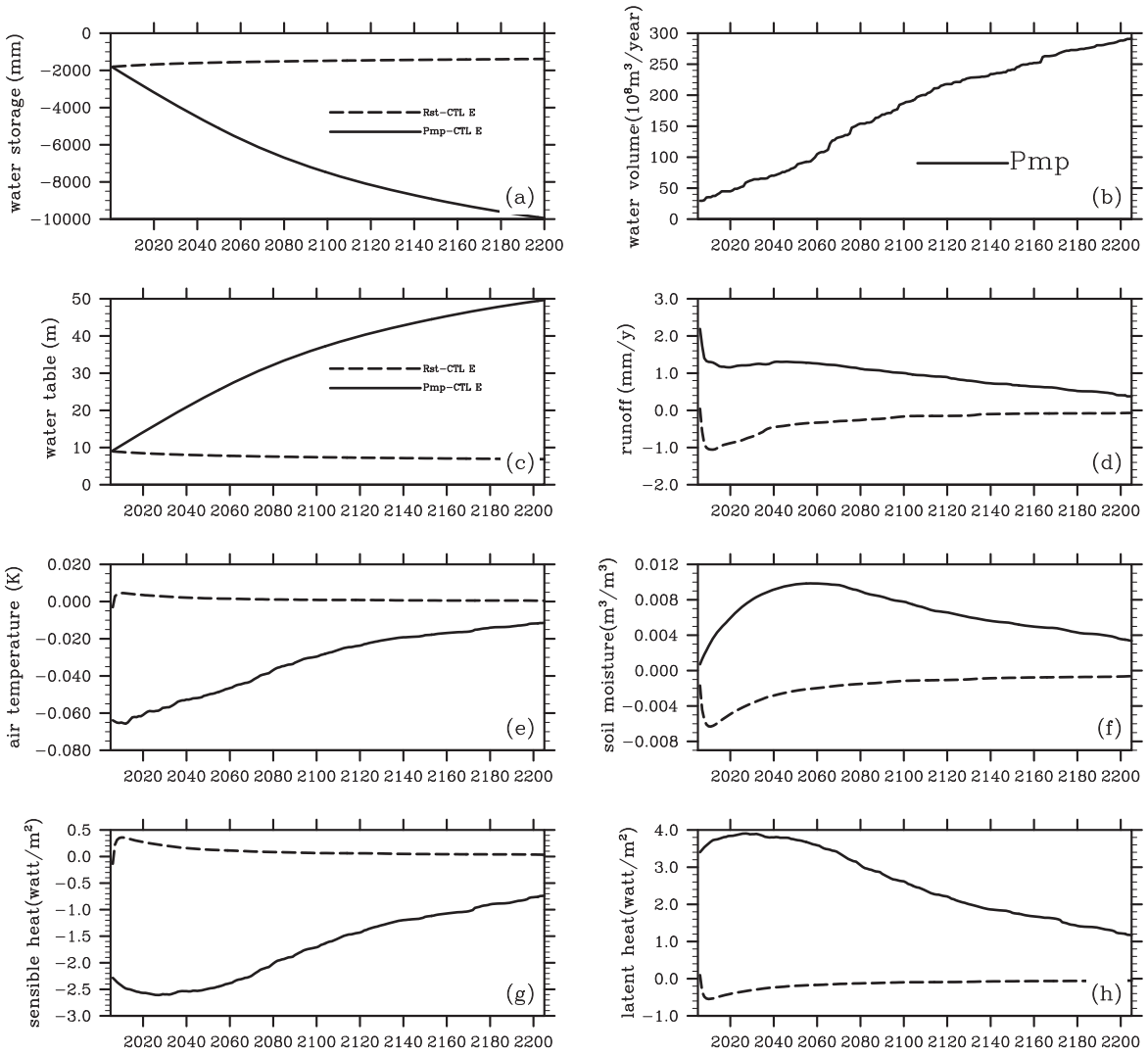

Fig. 12. Time series of (a) land water storage differences; (b) total water deficiency in the Pmp test; (c) groundwater table differences; (d) total runoff differences; (e) 2 m air temperature differences; (f) total soil moisture differences; (g) sensible heat flux differences; (h) latent heat flux differences in the Pmp, Rst, and CTL_E tests.

the aquifers but also to the dry climate forcing that does not favor increasing land water storage. The total runoff (Fig. 12d) in the Pmp test was still be greater than that in the control test, and the difference in runoff between the Pmp and CTL_E simulations declined continuously in subsequent years, because less water was then available for irrigation. The difference between the 2 m air temperatures simulated with Pmp and CTL_E (Fig. 12e) decreased gradually but still remained about 0.01 K colder after 200 years. From the total soil moisture difference shown in Fig. 12f, the wetting effect continued to increase in the first 50 years, but started to decrease over time as the groundwater resource dwindled. The energy flux differences in Fig. 12g and h behaved similarly to soil moisture but the greatest differences emerged in 2030, earlier than in the soil moisture because of the rapider responses of the energy flux.

For the recovery scenario Rst, in which the exploitation process was abruptly stopped, some negative effects emerged within the first 10 years, such as reduced soil moisture, increased temperature, and reduced runoff, compared with the cooling and wetting effects in the historic water-pumping simulations. The differences between the variables for the Rst and CTL_E tests—in air temperature, soil moisture, runoff, and so on—tended toward zero in the following hundreds of years. However, groundwater storage was not included. The rates of change differed among the moisture and energy amounts and fluxes. If we define $\left|\frac{m_{i+1}-m_i}{\overline{m}}\right| < 0.001$ (where m is the variable, and i is the year index) as the signal that the differences between the Rst and CTL_E tests have reached a constant value, the years in which the differences became constant were 2046 for 2 m air temperature, 2078 for sensible heat, 2101 for total runoff, 2144 for latent heat, and 2183 for soil moisture. The differences in the groundwater table and water storage did not become constant within the 200-year simulation period because there restoration rates are slow. The years in which the differences became constant for these moisture and energy variables depended on their own rates of change.

Fig. 13 shows the spatial distributions of the groundwater table, soil moisture, sensible heat flux, and latent heat flux in 2050 and 2200. Generally, the spatial distributions in the two future hypothetical tests (Pmp and Rst) did not differ greatly from the results in the historical tests, except in the magnitudes of the changes. This was because the water demands did not change in the future tests. In the Pmp test, the groundwater table continued to decline. At the end of the simulation period in 2200, the groundwater table in the plain areas (Fig. 13c) had almost reached the

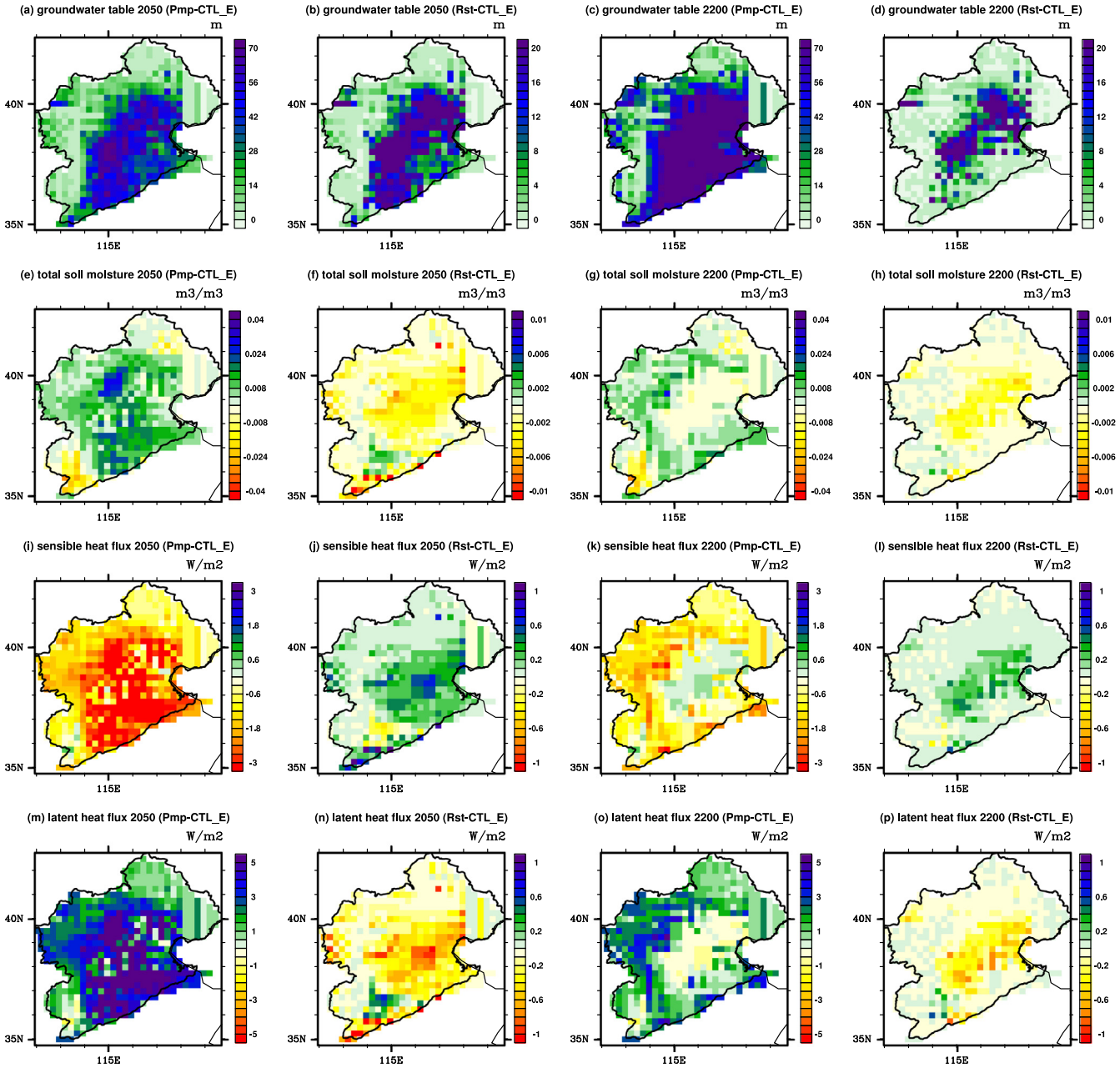

Fig. 13. Spatial distributions of (a) groundwater table in 2050 (Pmp – CTL_E); (b) groundwater table in 2050 (Rst – CTL_E); (c) groundwater table in 2200 (Pmp – CTL_E); (d) groundwater table in 2200 (Rst – CTL_E); (e) total soil moisture in 2050 (Pmp – CTL_E); (f) total soil moisture in 2050 (Rst – CTL_E); (g) total soil moisture in 2200 (Pmp – CTL_E); (h) total soil moisture in 2200 (Rst – CTL_E); (i) sensible heat flux in 2050 (Pmp – CTL_E); (j) sensible heat flux in 2050 (Rst – CTL_E); (k) sensible heat flux in 2200 (Pmp – CTL_E); (l) sensible heat flux in 220 (Rst – CTL_E); (m) latent heat flux in 2050 (Pmp – CTL_E); (n) latent heat flux in 2050 (Rst – CTL_E); (o) latent heat flux in 2200 (Pmp – CTL_E); and (p) latent heat flux in 2200 (Rst – CTL_E).

maximum depth of 80 m. Unlike the groundwater table, the changes in the other variables increased in the early years of the simulation period, but subsequently became small over time. The wetting and cooling changes on the land surface reached their maximum values in the years around 2050 (Fig. 13e, i, and m). In 2200, the changes (Fig. 13g, k, and o) were clearly smaller than those in 2050. In the central and eastern areas of the Basin, where the groundwater table reached the depth of the bedrock first, the moisture and energy amounts and fluxes approached the level in the control test. In the other areas, the process of exploitation did not cease and the wetting and cooling effects persisted. In the Rst test, drying and warming effects emerged in the whole Basin, with the greatest changes in the central and eastern plain areas. Although these changes were rather small, the dry and warm changes in the plain areas still persisted in 2200 (Fig. 13h, l, and p).

Fig. 14 shows the results of future simulations from 2001 to 2100 driven by future climate scenario data. Despite greater inter-annual variations, the changes in the variables in Fig. 14 are similar to those in Fig. 12. In the Pmp_F test, the wetter forcing of the future climate data means that the water storage and groundwater table in Fig. 14a and c do not decline as rapidly as they did in the Pmp simulation, with constant historical climate data. The total water deficiency shown in Fig. 14b also increases with the years, but more slowly. The total runoff generated and the total soil

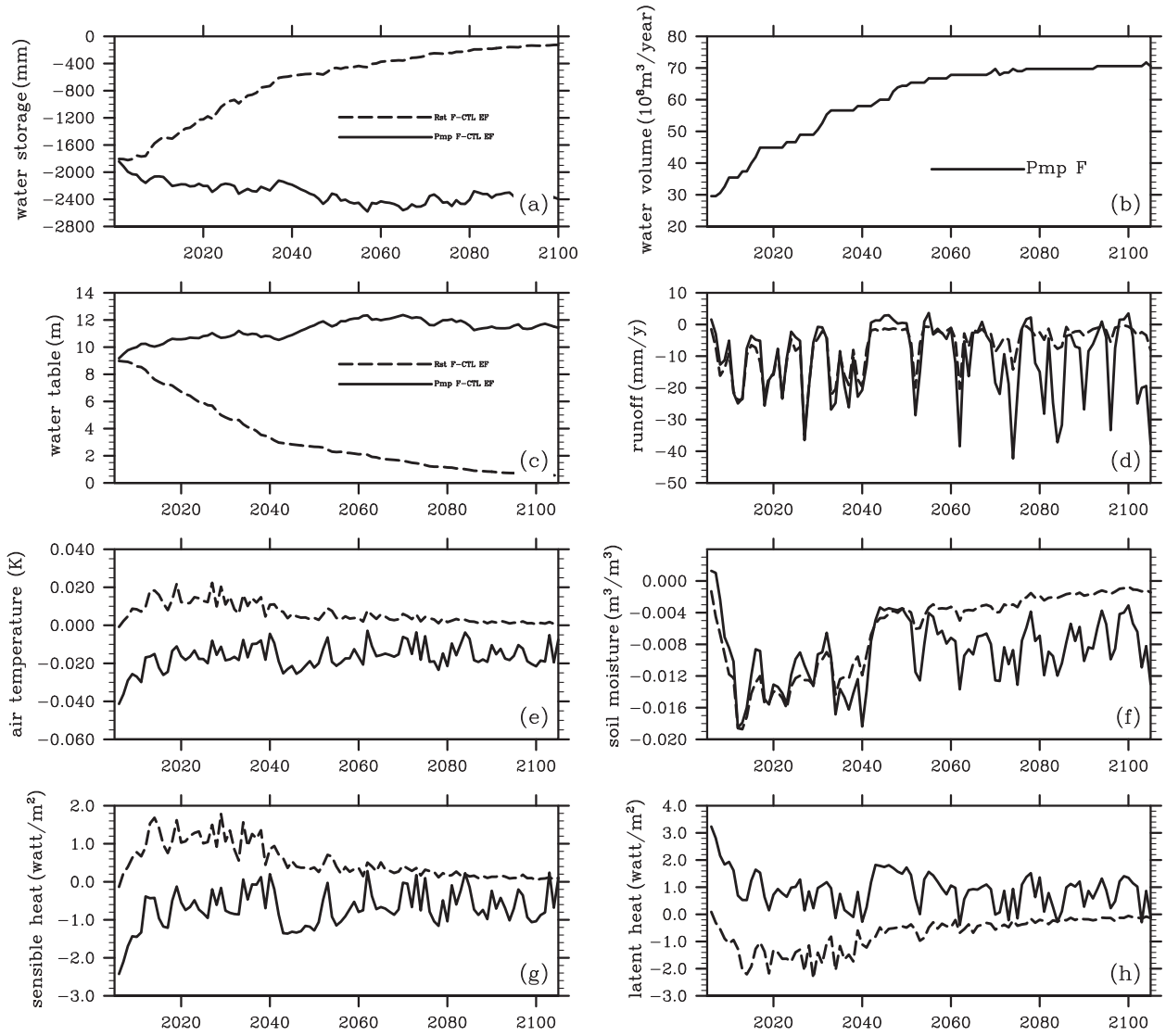

Fig. 14. Time series of (a) land water storage differences; (b) total water deficiency in the Pmp_F test; (c) groundwater table differences; (d) total runoff differences; (e) 2 m air temperature differences; (f) total soil moisture differences; (g) sensible heat flux differences; and (h) latent heat flux differences in the Pmp_F, Rst_F, and CTL_EF tests.

moisture in the Pmp_F test were lower than those in the CTL_EF test, which differs slightly from the results of the Pmp and CTL_E tests. This is probably because the difference in the top soil moisture between the Pmp_F and CTL_EF simulations was relatively small because precipitation was heavy. The increase in surface runoff attributable to irrigation was therefore small in the Pmp_F test, but the groundwater exploitation process still constrained the generation of subsurface runoff. The changes in temperature and heat fluxes shown in Fig. 14 are similar to those in Fig. 12—that is, the reductions in temperature and increases in latent heat flux weakened over the years of the simulation. In the Rst_F test, the changes were very similar to the results of the Rst simulation. The natural restoration of the groundwater resource led to a rise in the groundwater table, whereas warmer and drier effects emerged in the early decades of the simulations and then weakened gradually. Compared with the Pmp, Rst, and CTL_E tests, the results of the Pmp_F, Rst_F, and CTL_EF simulations indicated that no matter what the future climate is like, the changing trends of moisture and energy amounts and fluxes in the three cases will be almost the same, despite their different rates and degrees of change.

5. Discussion and conclusions

In this study, a simple conceptual scheme of anthropogenic water resource exploitation was implemented into the land surface model CLM3.5 to explore the effects of human-induced land water resource exploitation and use on land surface processes. The Haihe River Basin in northern China, which is facing water resource overexploitation, was chosen as the study domain. Historical simulations from 1965 to 2000 with different water demands, and future simulations were conducted to investigate the effects of water overexploitation and the possible responses to different exploitation scenarios in the Basin. The main conclusions of this study are as follows. (1) Groundwater exploitation and utilization has brought about cooling and wetting changes at the land surface, accompanied by reduced land water resources in the Basin, including a lowered groundwater table, reduced temperature, enhanced latent heat flux, increased surface runoff, etc. These changes are positively related to the different water demands. (2) If water exploitation is to continue at the rate observed in 2000, the cooling and wetting changes caused by groundwater exploitation and utilization will weaken as the local groundwater resources are

exhausted and exploitation ceases. (3) If exploitation is stopped immediately to allow the water resources to recover, negative changes will emerge in the Basin over the first 10 years: reduced soil moisture, reduced runoff, and increased 2 m air temperature. These differences will then disappear gradually by the end of the simulation period, except for the slow restoration of the groundwater, which will take much longer. (4) The two hypothetical scenarios (continued exploitation at the current rate or complete cessation) simulated for the future provide us with evidence that the local land water resources cannot continue to supply the current overexploitation processes in the long term. Because natural water resources cannot be replenished quickly, the water demand must be reduced to achieve a balance between slow restoration and rapid exploitation, if social long-term stability and development are to be maintained. Some measures should be adopted to achieve sustainable development in the Basin, including popularizing water-saving technologies, publicizing and establishing public awareness of the need to save water, and urging a transition from high-water-consumption to low-water-consumption industries. (5) The increased water-use expense and subsequent ecological deterioration due to groundwater overexploitation may further lead to reduced food production and slowing industry. These negative effects seriously threaten social sustainable development and make the region less livable in the future.

We note that many assumptions made in this study add uncertainties and reduce the accuracy of our results, which should be mentioned and addressed. First, estimation of the water demands in the simulation tests greatly simplifies the whole process of water exploitation and consumption. The lack of seasonal variations in irrigation may have led to an underestimation of the water consumed and a flattening of the wetting and cooling effects in the irrigation season. When considering domestic and industrial consumption, the proportion of wastewater returned to the rivers was subjectively set. It is based only on a small-scale survey (Mao et al., 2000), and more effective evidence is required in the future. Second, processes not represented in the CLM land surface model, such as the effects of lakes, reservoirs and lateral groundwater flow, add uncertainties to the simulations. Also, the uniformed parameters in CLM may introduce uncertainties during simulations over some particular basins. Third, simulation levels of the CLM rely largely on the forcing atmospheric data, as demonstrated by Wang and Zeng (2011).

We tried to investigate how water resource exploitation and consumption affects the land surface, and to discuss the sensitivity of these effects to different water demands. We hope that this study will provide useful information to allow policy makers to better understand the relationship between water resource exploitation and social development.

Acknowledgments

This study was supported by the National Natural Science Foundation of China with Grant 91125016, the Chinese Academy of Sciences Strategic Priority Research Program with Grant XDA05110102, and the National Basic Research Program of China with Grants 2010CB428403. We would like to thank the editor, Dr. Konstantine P. Georgakakos, and two anonymous reviewers for their comments and suggestions about this paper. We also thank Drs. Xiangjun Tian, Xiaoduo Pan, and Yingdong Yu for their assistance with data processing and for discussions about the results.

References

Adegoke, J.O., Pielke, R.A., Eastman, J., Mahmood, R., Hubbard, K.G., 2003. Impact of irrigation on midsummer surface fluxes and temperature under dry synoptic conditions: a regional atmospheric model study of the US high plain. Mon. Weather Rev. 131 (3), 556–564.

Alley, W.M., Healy, R.W., LaBaugh, J.W., Reilly, T.E., 2002. Flow and storage in groundwater system. Science 296, 1985–1990.

Chen, X., Hu, Q., 2004. Groundwater influences on soil moisture and surface evaporation. J. Hydrol. 297, 285–300.

Chen, F., Xie, Z., 2010. Effects of interbasin water transfer on regional climate: a case study of the middle route of the south-to-north water transfer project in China. J. Geophys. Res. 115, D11112. http://dx.doi.org/10.1029/2009JD012611.

Chen, X.H., Burbach, M., Cheng, C., 2008. Electrical and hydraulic vertical variability in channel sediments and its effects on streamflow depletion due to groundwater extraction. J. Hydrol. 352 (3–4), 250–266.

Chen, D., Ou, T., Gong, L., Xu, C., Li, W., Ho, C., Qian, W., 2010. Spatial interpolation of daily precipitation in China: 1951–2005. Adv. Atmos. Sci. 27 (6), 1221–1232. http://dx.doi.org/10.1007/s00376-010-9151-y.

Collins, W.D., Bitz, C.M., Blackmon, M.L., Bonan, G.B., Bretherton, C.S., Carton, J.A., Chang, P., Doney, S.C., Hack, J.J., Henderson, T.B., Kiehl, J.T., Large, W.G., McKenna, D.S., Santer, B.D., Smith, R.D., 2006. The community climate system model version 3 (CCSM3). J. Climate 19 (11), 2122–2143.

DeAngelis, A., Dominguez, F., Fan, Y., Robock, A., Kutsu, M.D., Robinson, D., 2010. Evidence of enhanced precipitation due to irrigation over the great plains of the United States. J. Geophys. Res. 115, D15115. http://dx.doi.org/10.1029/2010JD013892.

Department of Urban & Social Economic Survey, National Bureau of Statistics of China, 2001. Urban Statistical Yearbook of China 2000. China Statistics Press, Beijing (in Chinese).

Döll, P., Hoffmann-Dobrev, H., Portmann, F.T., Siebert, S., Eicker, A., Rodell, M., Strassberg, G., Scanlon, B.R., 2012. Impact of water withdrawals from groundwater and surface water on continental water storage variations. J. Geodyn. 59–60, 143–156.

Fei, Y., Li, H., Shen, J., 2006. Evolution situation and sustainable utilization prospects of groundwater resource in Haihe River Valley. Acta Geosci. Sin. 22 (4), 298–301 (in Chinese).

Haddeland, I., Lettenmaier, D.P., Skaugen, T., 2006. Effects of irrigation on the water and energy balances of the Colorado and Mekong river basins. J. Hydrol. 324, 210–223.

Hanasaki, N., Kanae, S., Oki, T., Masuda, K., Motoya, K., Shirakawa, N., Shen, Y., Tanaka, K., 2008. An integrated model for the assessment of global water resources – Part 1: Model description and input meteorological forcing. Hydrol. Earth Syst. Sci. 12, 1007–1025.

Huang, M., Hou, Z., Leung, L.R., Ke, Y., Liu, Y., Fang, Z., Sun, Y., 2013. Uncertainty analysis of runoff simulations and parameter identifiability in the community land model: evidence from MOPEX basins. J. Hydrometeorol. 14, 1754–1772.

Jia, Y., Ding, X., Wang, H., Zhou, Z., Qiu, Y., Niu, C., 2012. Attribution of water resources evolution in the highly water-stressed Hai River Basin of China. Water Resour. Res. 48, W02513. http://dx.doi.org/10.1029/2010WR009275.

Kollet, S.J., Zlotnik, V.A., 2003. Stream depletion predictions using pumping tests data from a heterogeneous stream-aquifer system (a case study from the Great Plains, USA). J. Hydrol. 281 (1–2), 96–114.

Konikow, L.F., Kendy, E., 2005. Groundwater depletion: a global problem. Hydrogeol. J. 13 (1), 317–320.

Koster, R.D., Suarez, M.J., 2001. Soil moisture memory in climate models. J. Hydrometeorol. 2, 558–570.

Kueppers, L.M., Snyder, M.A., Sloan, L.C., 2007. Irrigation cooling effect: regional climate forcing by land use change. Geophys. Res. Lett. 34, L03703. http://dx.doi.org/10.1029/2006GL028679.

Kustu, M.D., Fan, Y., Robock, A., 2010. Large-scale water cycle perturbation due to irrigation pumping in the US high plains: a synthesis of observed streamflow changes. J. Hydrol. 390 (1–4), 222–244.

Liang, F., Tao, S., Wei, J., Bueh, C., 2011. Variation in summer rainfall in north China during the period 1956–2007 and links with atmospheric circulation. Adv. Atmos. Sci. 28 (2), 363–374. http://dx.doi.org/10.1007/s00376-010-9220-2.

Liu, J., Zheng, C., Lei, Y., 2008. Ground water sustainability: methodology and application to the north China plain. Ground Water 46 (6), 897–909.

Mao, X., Ni, J., Guo, Y., 2000. A case study on characteristics of wastewater effluents in accelerated economic growth areas. Acta Sci. Circum. 20 (2), 219–224 (in Chinese).

Niu, G., Yang, Z., Dickinson, R.E., Gulten, L.E., 2005. A simple TOPMODEL-based runoff parameterization (SIMTOP) for use in global climate models. J. Geophys. Res. 110, D21106. http://dx.doi.org/10.1029/2005JD006111.

Niu, G., Yang, Z., Dickinson, R.E., Gulten, L.E., Su, H., 2007. Development of a simple groundwater model for use in climate models and evaluation with gravity recovery and climate experiment data. J. Geophys. Res. 112, D07103. http://dx.doi.org/10.1029/2006JD007522.

Oleson, K.W., Dai, Y., Bonan, G., Bosilovich, M., Dickinson, R., Dirmeyer, P., Hoffman, F., Houser, P., Levis, S., Niu, G., Thornton, P., Vertenstein, M., Yang, Z., Zeng, X., 2004. Technical description of the community land model (CLM), Tech. Rep. Technical Note NCAR/TN-461+STR, NCAR.

Oleson, K.W., Niu, G., Yang, Z., Lawrence, D.M., Thornton, P.E., Lawrence, P.J., Stockli, R., Dickinson, R.E., Bonan, G.B., Levis, S., Dai, A., Qian, T., 2008. Improvements to the community land model and their impact on the hydrological cycle. J. Geophys. Res. 113, G01021. http://dx.doi.org/10.1029/2007JG000563.

Ozdogan, M., Rodell, M., Beaudoing, H.K., Toll, D.L., 2010. Simulating the effects of irrigation over the United Sates in a land surface model based on satellite-derived agricultural data. J. Hydrometeorol. 11, 171–184.

Pokhrel, Y., Hanasaki, N., Koirala, S., Cho, J., Yeh, P.J.-F., Kim, H., Kanae, S., Oki, T., 2012. Incorporating anthropogenic water regulation modules into a land surface model. J. Hydrometeorol. 13, 255–269.

Ran, Y., Li, X., Lu, L., Li, Z., 2012. Large-scale land cover mapping with the integration of multi-source information based on the Dempster–Shafer theory. Int. J. Geogr. Inf. Sci. 1–23. http://dx.doi.org/10.1080/13658816.2011.577745.

Ren, X., 2007. Water Resource Assessment of Haihe River Basin. China WaterPower Press, Beijing (in Chinese).

Ren, L., Wang, M., Li, C., Zhang, W., 2002. Impacts of human activity on river runoff in the northern area of China. J. Hydrol. 261, 204–217.

Rodell, M., Velicogna, I., Famiglietti, J., 2009. Satellite-based estimates of groundwater depletion in India. Nature 460, 999–1002.

Sakaguchi, K., Zeng, X., 2009. Effects of soil wetness, plant litter, and under-canopy atmospheric stability on ground evaporation in the community land model (CLM3.5). J. Geophys. Res. 114, D01107. http://dx.doi.org/10.1029/2008JD010834.

Sha, T., Roy, A.D., Qureshi, A.S., Wang, J., 2003. Sustaining Asia's groundwater boom: an overview of issues and evidence. Nat. Resour. Forum 27, 130–141.

Sheffield, J., Goteti, G., Wood, E.F., 2006. Development of a 50-yr high resolution global dataset of meteorological forcings for land surface modeling. J. Climate 19 (13), 3008–3111.

Szilagyi, J., 1999. Streamflow depletion investigations in the Republican River basin: Colorado, Nebraska, and Kansas. J. Environ. Syst. 27 (3), 251–263.

Szilagyi, J., 2001. Indentifying cause of declining flows in the Republican River. J. Water Resour. Plan. Manage. 127 (4), 244–253.

Tapley, B.D., Bettadpur, S., Ries, J., Thompson, P.F., Watkins, W.W., 2004. GRACE measurements of mass variability in the earth system. Science 305, 503–505.

Taylor, K.E., Stouffer, R.J., Meehl, G.A., 2012. An overview of CMIP5 and the experiment design. Bull. Am. Meteorol. Soc. 93, 485–498.

Tian, X., Xie, Z., Dai, A., 2008. A land surface soil moisture data assimilation system based on the dual-UKF method and the community land model. J. Geophys. Res. 113, D14127. http://dx.doi.org/10.1029/2007JD009650.

Wada, Y., van Beek, L.P.H., van Kempen, C.M., Reckman, J.W.T.M., Vasak, S., Bierkens, M.F.P., 2010. Global depletion of groundwater resources. Geophys. Res. Lett. 37, L20402. http://dx.doi.org/10.1029/2010GL044571.

Wada, Y., van Beek, L.P.H., Bierkens, M.F.P., 2012. Nonsustainable groundwater sustaining irrigation: a global assessment. Water Resour. Res. 48 (W00L06). http://dx.doi.org/10.1029/2011WR010562.

Wang, A., Zeng, X., 2011. Sensitivities of terrestrial water cycle simulations to the variations of precipitation and air temperature in China. J. Geophys. Res. 116, D02107. http://dx.doi.org/10.1029/2010JD014659.

Wei, Y., Miao, H., Ouyang, Z., Wang, X., 2006. Ensure measures of water balance and ecological water needs in Haihe Basin. J. Water Resour. Water Eng. 17 (1), 11–14 (in Chinese).

Wen, F.J., Chen, X.H., 2006. Evaluation of the impact of groundwater irrigation on streamflow depletion in Nebraska. J. Hydrol. 327, 603–617.

Xia, J., Chen, D., 2001. Water problem and opportunities in hydrological sciences in China. Hydrol. Sci. J. 46 (6), 907–922.

Xia, J., Zhang, Y., 2008. Water security in north China and countermeasure to climate change and human activity. Phys. Chem. Earth 33, 359–363.

Xu, Y., Mo, X., Cai, Y., Li, X., 2004. Analysis on groundwater table drawdown by land use and quest for sustainable water use in the Hebei Plain in China. Agric. Water Manage. 75, 38–53.

Yang, Y., Tian, F., 2009. Abrupt change of runoff and its major driving factors in Haihe River Catchment, China. J. Hydrol. 374, 373–383.

Yuan, X., Xie, Z., Zheng, J., Tian, X., Yang, Z., 2008. Effects of water table dynamics on regional climate: a case study over east Asian monsoon area. J. Geophys. Res. 113, D21112. http://dx.doi.org/10.1029/2008JD0101.

Zou, J., Xie, Z., Yu, Y., Zhan, C., Sun, Q., 2014. Climatic responses to anthropogenic groundwater exploitation: a case study of the Haihe River Basin, northern China. Clim. Dyn. 42, 2125–2145. http://dx.doi.org/10.1007/s00382-013-1995-2.